

# *Development and optimization of solid lipid nanoparticles coated with chitosan and poly(2-ethyl-2-oxazoline) for ocular drug delivery of ciprofloxacin*

Article

Published Version

Creative Commons: Attribution 4.0 (CC-BY)

Open access

Onugwu, A. L., Attama, A. A., Nnamani, P. O., Onugwu, S. O., Onuigbo, E. B. and Khutoryanskiy, V. V. ORCID: <https://orcid.org/0000-0002-7221-2630> (2022) Development and optimization of solid lipid nanoparticles coated with chitosan and poly(2-ethyl-2-oxazoline) for ocular drug delivery of ciprofloxacin. *Journal of Drug Delivery Science and Technology*, 74. 103527. ISSN 1773-2247 doi: <https://doi.org/10.1016/j.jddst.2022.103527> Available at <https://centaur.reading.ac.uk/105849/>

It is advisable to refer to the publisher's version if you intend to cite from the work. See [Guidance on citing](#).

Published version at: <https://www.sciencedirect.com/science/article/pii/S1773224722004385#!>

To link to this article DOI: <http://dx.doi.org/10.1016/j.jddst.2022.103527>

Publisher: Elsevier

All outputs in CentAUR are protected by Intellectual Property Rights law, including copyright law. Copyright and IPR is retained by the creators or other copyright holders. Terms and conditions for use of this material are defined in

the [End User Agreement](#).

[www.reading.ac.uk/centaur](http://www.reading.ac.uk/centaur)

## **CentAUR**

Central Archive at the University of Reading

Reading's research outputs online



# Development and optimization of solid lipid nanoparticles coated with chitosan and poly(2-ethyl-2-oxazoline) for ocular drug delivery of ciprofloxacin

Adaeze L. Onugwu<sup>a,b</sup>, Anthony A. Attama<sup>a,c,\*\*</sup>, Petra O. Nnamani<sup>a</sup>, Sabastine O. Onugwu<sup>d</sup>, Ebele B. Onuigbo<sup>c,e</sup>, Vitaliy V. Khutoryanskiy<sup>b,\*</sup>

<sup>a</sup> Drug Delivery and Nanomedicines Research Laboratory, Department of Pharmaceutics, University of Nigeria, Nsukka, 410001, Enugu State, Nigeria

<sup>b</sup> Reading School of Pharmacy, University of Reading, Whiteknights, Reading, RG6 6AD, United Kingdom

<sup>c</sup> Institute for Drug, Herbal Medicine and Excipient Research and Development, University of Nigeria, Nsukka, Enugu State, Nigeria

<sup>d</sup> Department of Pharmacognosy, Enugu State University of Science and Technology, Enugu State, Nigeria

<sup>e</sup> Department of Pharmaceutical Microbiology and Biotechnology, University of Nigeria, Nsukka, 410001, Enugu State, Nigeria

## ARTICLE INFO

### Keywords:

Solid lipid nanoparticles  
poly(2-ethyl-2-oxazoline)  
Chitosan  
Box-behnken design  
Ciprofloxacin  
Ocular delivery

## ABSTRACT

Many formulation strategies have been employed to improve ocular bioavailability of topical eye drops. The aim of this study was to develop and evaluate a series of solid lipid nanoparticles coated with poly(2-ethyl-2-oxazoline) and chitosan for ocular delivery of ciprofloxacin. Ciprofloxacin-loaded poly(2-ethyl-2-oxazoline) (PSLN) formulation was prepared by a combination of melt-emulsion sonication and low-temperature solidification methods. A Box-Behnken design, was employed to statistically optimize the effects of the amount of drug ( $X_1$ ), lipid:polymer ratio ( $X_2$ ) and surfactant concentration ( $X_3$ ) on particle size ( $Y_1$ ) and entrapment efficiency ( $Y_2$ ). Analysis of variance was used to validate the optimization design; and regression equations and response surface plots were generated. The optimized formulation was selected through numerical point prediction approach. These nanoparticles were characterized using dynamic light scattering, transmission electron microscopy (TEM), differential scanning calorimetry (DSC), and powder X-ray diffractometry (PXRD). *In vitro* drug release and corneal permeation studies were carried out, while the mucoadhesive properties were evaluated *in vivo* using porcine corneal tissue. The particle size and zeta potential of the optimized formulations ranged from 141 to 213 nm and +24.6 to -35.6 mV, respectively. PSLN possessed higher encapsulation efficiency than chitosan-coated solid lipid nanoparticles (CSLN). The *in vitro* drug release from all the formulations showed an initial burst release followed by prolonged release over 24 h. The release mechanism followed Korsmeyer-Peppas model and Fickian diffusion ( $n < 0.5$ ). DSC revealed lower enthalpy and crystallinity of the formulations as also detected by PXRD, while TEM showed spherical particles in the lower nanometer range with a layer of polymer coating. The results of this study demonstrated that CSLN exhibited higher mucoadhesion and retention on corneal tissues compared with PSLN and also showed higher flux and apparent permeability, but with lower entrapment efficiency.

## 1. Introduction

Ocular infections are basically treated by using topical application of antibiotics in the form of eye drops. Topical administration is the preferred route for ocular drug delivery because of its simplicity and non-invasiveness; and it represents 90% of the commercial dosage forms

used in eye care [1]. The primary goal of topical ocular delivery is to treat diseases affecting the ocular surface such as conjunctivitis, blepharitis, and keratoconjunctivitis within the anterior segment of the eye. There is also a goal for the administered drug to penetrate through the cornea to treat intraocular pathologies, such as glaucoma and uveitis [2]. However, there are some anatomical and physiological constraints

\* Corresponding author.

\*\* Corresponding author. Drug Delivery and Nanomedicines Research Laboratory, Department of Pharmaceutics, University of Nigeria, Nsukka, 410001, Enugu State, Nigeria.

E-mail addresses: [anthony.attama@unn.edu.ng](mailto:anthony.attama@unn.edu.ng) (A.A. Attama), [v.khutoryanskiy@reading.ac.uk](mailto:v.khutoryanskiy@reading.ac.uk) (V.V. Khutoryanskiy).

<https://doi.org/10.1016/j.jddst.2022.103527>

Received 9 February 2022; Received in revised form 12 June 2022; Accepted 15 June 2022

Available online 22 June 2022

1773-2247/© 2022 The Authors. Published by Elsevier B.V. This is an open access article under the CC BY license (<http://creativecommons.org/licenses/by/4.0/>).

to drug absorption imposed by the structure of the eye. Due to these constraints, about 90% of the dose applied topically through eye drops is usually lost through lacrimation and nasolacrimal drainage [3]. To achieve adequate drug levels in the eye tissues, frequent dosing is required leading to adverse drug effects, poor patient compliance and possible antibiotic resistance.

To circumvent these limitations of conventional eye drops, there is an increasing interest in the concept of “modified eye drops” based on nanotechnology such as lipid nanoparticles [4–6]. When compared to other colloidal systems, lipid nanoparticles have been described as superior carriers [7]. Lipid nanoparticles include solid lipid nanoparticles (SLNs), nanostructured lipid carriers, lipid-drug conjugates, and lipid-polymer nanoparticles. SLNs are made up of a solid lipid core entrapping drug stabilized by a layer of surfactants. SLNs are biocompatible and non-toxic as they are prepared from physiological and biodegradable lipids [8]. The interaction of the lipid component of the lipid nanoparticles with the lipid layer of the tear film leads to retention of the delivery system in the conjunctiva sac, where it serves as a drug depot [9,10]. Their nanosize, high viscosity and composition also contribute to their high corneal retention and permeability profile. All these features of SLNs enhance the transcorneal drug delivery and prolong the pre-corneal retention in the conjunctival sac, which increases the ocular bioavailability of drugs.

SLNs can be modified by coating with cationic materials such as chitosan or with polyethylene glycol (commonly known as PEGylation) to improve their pharmacokinetic profile. The primary purpose of surface modification is to maximize or to minimize the interaction of the nanoparticles with the ocular surface and promote nanoparticle mucoadhesion or penetration. Surface modification with cationic and mucoadhesive material like chitosan increases electrostatic interactions between positively charged nanoparticles and the negatively charged surface of the cornea [11,12]. This improves drug residence in the ocular surface through mucoadhesion. Some researchers have also reported the ability of chitosan to reversibly disrupt corneal epithelial tight junctions which can lead to improved permeability of chitosan coated nanoparticles through the cornea [13,14].

The use of poly(ethylene glycol) (PEG), otherwise known as PEGylation, as a mean of providing stealth properties to the nanoparticles, is not new in drug delivery technology. The hydrophilic polymer stealth layer surrounding the lipid shell in PEGylated SLNs enhances nanoparticle stability and circulation lifetime [15]. The structure of PEGylated SLN provides the opportunity to load multiple drugs of different physicochemical properties. It is also associated with the benefits of drug targeting and controlled release at the site of action. PEG is the most widely used “stealth” polymer in drug delivery [16]. However, PEG has some limitations, and so there is a need to consider alternative polymers [17]. Some poly(2-alkyl-2-oxazolines) have been reported to exhibit stealth-like properties similar to PEG, and they have many advantages over PEG [18,19]. These advantages include their non-toxicity, ease of preparing polymers with different functionalities, a high degree of renal clearance with no bioaccumulation, and stability against oxidative degradation [20–22]. Poly (2-alkyl-2-oxazolines) are synthesized from readily available monomers. Some poly(2-alkyl-2-oxazolines) are soluble in water and in some other common polar organic solvents.

The present study was designed to develop, optimize and compare ciprofloxacin-loaded solid lipid nanoparticles coated with chitosan (CSLN) and poly(2-ethyl-2-oxazoline) (POZylated SLN, PSLN) by using different ratios of lipid and polymer through the statistical design expert approach – Box-Behnken design (BBD). Ciprofloxacin (CIP) was selected as the model drug because of its potential benefits in the treatment of anterior segment eye infections. After screening for formulation parameters that affect the quality of PSLN formulation, BBD was used to investigate the individual and interaction effects of the weight of drug, lipid/polymer ratio and surfactant on particle size and entrapment efficiency of PSLN. An optimized PSLN was obtained using the predicted optimum levels of the formulation parameters. CIP-loaded SLN (SLN)

and chitosan coated SLN (CSLN) were also prepared using the same method for comparison. The physicochemical properties, release profiles, mucoadhesion and corneal permeation properties of optimized PSLN, SLN and CSLN were investigated.

## 2. Materials and methods

### 2.1. Materials

Ciprofloxacin, Tween® 80, poly(2-ethyl-2-oxazoline) (average Mw ~50,000 Da, PDI 3–4), chitosan (low molecular weight), fluorescein sodium, FITC-dextran, acetone and absolute ethanol (>99.8%) were purchased from Sigma-Aldrich (Gillingham, UK). Compritol® ATO 888 was kindly provided by Gattefossé (St. Priest, France). All the other reagents and solvents were of analytical grade. The porcine corneas used in this study were obtained from P.C. Turner Abattoir (Hampshire, UK).

### 2.2. Methods

#### 2.2.1. Response surface design

After the identification of the factors that affect the quality of the SLN in the preliminary study, a response surface methodology (RSM) design was used to statistically investigate the effects of these parameters on selected responses. BBD, a 3-factor, 3-level design, was used to optimize the independent variables and to evaluate both the main and interaction effects on the dependent variables using Design-Expert 12.0.0.6 software (Stat-Ease Inc., Minneapolis, USA). The independent variables used were amount of drug, lipid/polymer ratio and surfactant concentration; and their effects on particle size and encapsulation efficiency were investigated. The dependent and independent variables selected for the POZylated SLN are shown in Table S1 along with their low (–1), medium (0) and high (+1) levels. These levels were selected based on the results of the preliminary experiments.

A total of 17 experimental runs were carried out. Twelve out of the 17 runs represent the mid-point of each edge of a cube and the remaining five runs are the replicates of the cube’s center point. Quadratic and linear models were generated as:  $Y_1 = b_0 + b_1X_1 + b_2X_2 + b_3X_3 + b_{12} \times 1 \times 2 + b_{13} \times 1 \times 3 + b_{23} \times 2 \times 3 + b_{11} \times 1^2 + b_{22} \times 2^2 + b_{33} \times 3^2$  and  $Y_2 = b_0 + b_1X_1 + b_2X_2 + b_3X_3$  respectively; where  $Y_1$  and  $Y_2$  are the measured responses;  $b_0$  is constant;  $b_1, b_2, b_3$  are linear coefficients,  $b_{12}, b_{13}, b_{23}$  are interaction coefficients among three factors,  $b_{11}, b_{22}, b_{33}$  are quadratic coefficients of observed experimental values; and  $X_1, X_2$  and  $X_3$  are levels of independent variables. The responses were evaluated statistically using analysis of variance (ANOVA). Further, the optimum formulation was selected by the numerical point prediction.

#### 2.2.2. Preparation of PSLN, SLN and CSLN formulations

Ciprofloxacin loaded POZylated SLN (PSLN) were prepared by a combination of melt-emulsion sonication and low-temperature solidification methods [23,24]. Briefly, Compritol and poly(2-ethyl-2-oxazoline) (PEOx) were dispersed in 1 mL of 1:1 mixture of absolute ethanol and acetone, and then heated to 80 °C in a water bath. Appropriate amount of CIP was weighed out and dissolved in the molten lipid/polymer mixture. Aqueous surfactant solution (5 mL) heated to the same temperature as the lipid phase was added to the solution. The mixture was stirred on a magnetic stirrer at 400 rpm for 5 min and the coarse emulsion formed was sonicated using a probe sonicator (Fisherbrand 120, Fisher scientific, UK) at 60% amplitude for 5 min. The produced emulsion was added to chilled water (2–4 °C) and stirred using a magnetic stirrer for 30 min to yield a uniform dispersion of the nanoparticles.

For the SLN formulation, Compritol was used alone without PEOx. For chitosan coated SLN (CSLN), 0.5% solution of chitosan was prepared in 0.1% acetic acid solution. Chilled chitosan solution was used in place of chilled water. All other steps remained the same. Composition of the

formulations is shown in Table 1.

### 2.2.3. Characterization

**2.2.3.1. Particle size and zeta potential.** The size and the polydispersity index (PDI) of all the formulations were measured using a zetasizer (Zetasizer-Nano ZS, Malvern Instruments Ltd., U.K.) through dynamic light scattering technique. All samples were diluted by 100-fold with ultrapure water prior to the measurement. For size analysis, a measurement angle of 173° was used with the backscattering technique. Electrophoretic mobility measurements for the determination of the zeta potentials were performed using the same equipment. All measurements were performed in triplicate.

**2.2.3.2. Differential scanning calorimetry (DSC).** The excipients, physical mixtures of the excipients and lyophilized formulations were characterized by differential scanning calorimetry (DSC Q2000, TA instruments, USA). All the samples were weighed (3–15 mg) accurately and hermetically sealed in the aluminum pan; and an empty aluminum pan was used as a reference. The samples were heated at a rate of 10 °C/min from 40 to 300 °C under the inert atmosphere of nitrogen at a rate of 50 mL/min. Overlaid thermograms of drug, excipients, physical mixture, and formulations were recorded.

**2.2.3.3. Powdered X-ray diffraction (PXRD).** PXRD analysis was performed using powder X-ray diffractometer (D8 Powder Diffractometer, Bruker, US) for the pure excipients, physical mixtures of excipients and lyophilized formulations. All the PXRD patterns were recorded at ambient temperature at 2θ diffraction angle in a range of 5–65°. The *d* spacings of the main reflections of the materials were calculated using Bragg equation (equation (1)), while the crystallinity of the ciprofloxacin, Compritol, physical mixtures of the excipients and lyophilized formulations was calculated using equation (2) [25].

$$n\lambda = 2d\sin\theta \quad [1]$$

where  $\lambda$  is the wavelength of the incident X-ray beam,  $n$  is a positive integer which describes the order of the interference and  $\theta$  is the scattering angle. The parameter  $d$  is the interlayer spacing.

$$\text{Crystallinity (\%)} = \frac{\text{Area of crystalline peaks}}{\text{Area of all peaks (Crystalline + Amorphous)}} \times 100 \quad [2]$$

**2.2.3.4. Transmission electron microscopy.** The morphology of the nanoparticles was investigated using transmission electron microscope (TEM) (JEM-1010; JEOL Ltd, Tokyo, Japan) operating at 200 kV. One drop of the formulations was deposited on a carbon-coated copper grid stained with uranyl acetate. The grid was inserted into microscope using a holder and images were taken at 104,000× and 69,200× magnification.

**2.2.3.5. HPLC determination of ciprofloxacin.** A validated isocratic HPLC method was used for the analysis of ciprofloxacin with slight modification [26]. HPLC system (Agilent 1100 system, Agilent

Technologies, USA) was composed of a pump (Waters 1252, a binary pump, USA) equipped with an automated sampling system (Waters 717 PlusAutosampler, USA). The system was monitored by ChemStation software. The mobile phase consisted of an 80:20 mixture of 25 mM orthophosphoric acid (adjusted to pH 3 with triethanolamine) and methanol:acetonitrile (7:3). A reversed phase C18 column (5 μm particle size, 4.6 × 150 mm, Waters) was used; and was maintained at 25 °C during the analysis. The mobile phase flowed over the column at a rate of 1.5 mL/min and total run time of 10 min. All the samples were analyzed by injecting 20 μL of the sample and UV detector (Waters 2487 a Dual λ Absorbance detector, USA) was set at wavelength of 277 nm. The drug concentrations were quantified by analyzing the peak area.

**2.2.3.6. Determination of entrapment efficiency of the nanoparticle formulations.** The entrapment efficiency of the formulations was analyzed by ultracentrifugation method [27]. Samples were centrifuged in a centrifuge (Microcentaur, MSE, UK) at 13,000 rpm for 1 h. The free amount of ciprofloxacin in the supernatant was analyzed using HPLC. Percent drug entrapment efficiency of the nanoparticle formulations were calculated using equation (3).

$$\text{Entrapment efficiency (\%)} = \frac{\text{Total drug} - \text{Free drug}}{\text{Total drug}} \times 100 \quad [3]$$

### 2.2.4. In vitro release study

*In vitro* release studies of the optimized formulations were performed using the dialysis bag method [28]. Prior to the test, the dialysis bag (MWCO 12–14 kDa dialysis tubing, Medicell membrane, UK) was soaked in deionised water for 12 h. Artificial tear fluid (ATF) used as a release medium was prepared by dissolving 6.78 g NaCl, 2.18 g NaHCO<sub>3</sub>, 1.38 g KCl and 0.084 g of CaCl<sub>2</sub>·2H<sub>2</sub>O in 1 L of deionised water and the pH adjusted to 7.4 [48]. A 2 mL aliquot of the sample was placed into the dialysis bag tied at the two ends and placed into 25 mL of release medium. The set up was maintained at 37 ± 1 °C and magnetically stirred at 100 rpm. The release medium (1 mL) was withdrawn at fixed time intervals and the same volume of fresh medium was added to maintain sink condition. The amount of drug released was determined using HPLC.

### 2.2.5. Mechanism and kinetic of release studies

Zero-order, first-order, Higuchi and the Korsmeyer-Peppas models [29–31] were used to analyze the *in vitro* release data and to determine the best model that describes ciprofloxacin release from the formulations. Excel add-in DDSolver version 1 was used in fitting the release profiles to the kinetic models [32]. The model with the lowest Akaike information criterion (AIC), highest model selection criterion (MSC) and highest adjusted coefficient of determination (R<sup>2</sup><sub>adj</sub>) values was considered as the best model to describe the mechanism of release of ciprofloxacin from the nanoparticle formulations [33].

### 2.2.6. Mucoadhesion studies using porcine cornea

Mucoadhesion studies were performed according to previously reported method [34]. Fluorescein sodium-containing formulations were prepared by loading the formulations with 10 mg of fluorescein sodium in place of ciprofloxacin using the method described above. Fluorescein sodium-containing nanoparticle formulations and 0.5 mg/mL FITC-dextran solution were used as test samples and negative control respectively. Fluorescence microscope (Imager A1, Zeiss, Germany) with an AxioCam MRm Zeiss camera at 0.80 magnification with 30.0 ms exposure time and 1296 × 966 pixels was used to detect the fluorescence intensity and capture microscopy images. Freshly slaughtered pig head was transported from the abattoir to the laboratory within 2 h post-mortem where the corneas were carefully dissected and used for the mucoadhesion study. ATF was prepared and maintained at a temperature of 37 °C. A syringe (60 mL) was filled with ATF and attached to a pump. Background microscopy images were recorded for each cornea

**Table 1**

Composition of optimized PSLN, SLN and CSLN formulations.

Excipients	Optimized PSLN	SLN	CSLN
Ciprofloxacin (mg)	20	20	20
Compritol (mg)	150	150	150
Poly (2-ethyl-2-oxazoline) (mg)	150	–	–
1:1 Ethanol/acetone (mL)	1	1	1
2% Tween 80 (mL)	5	5	5
Chilled water (g)	qs 20	qs 20	–
0.5% Chitosan solution (g)	–	–	qs 20

sample prior to the experiment. A 30  $\mu\text{L}$  volume of either fluorescently labelled nanoparticle formulation or control was placed onto the corneal surface, followed by 5 washing cycles, for each of which the cornea tissue was irrigated with 2 mL of ATF at a rate of 0.2 mL/min using a syringe pump. Fluorescence microscopy images were recorded immediately after the initial treatment and after each wash with the cornea tissue placed onto a glass slide. Each experiment was conducted in triplicate. Microscopy images were analyzed with ImageJ® software to get the fluorescence intensity (fluorescence, a. u.) after each wash and a plot of fluorescence intensity as a function of the volume of ATF used was presented. The mean fluorescence intensity values were normalized by subtracting the background fluorescence provided by the cornea tissue prior to exposing it to the test material and the initial (pre-wash) fluorescence was taken as an intensity of 100%.

### 2.2.7. Corneal permeation study

The corneas taken from freshly slaughtered pigs were carefully dissected along with 2–4 mm of surrounding sclera tissue from the eyeball and washed with cold saline so as to remove any adhering pigments. The washed cornea was preserved in freshly prepared phosphate buffer saline (pH 7.4) at 4 °C.

The fresh corneas obtained from the above procedure were mounted on the modified Franz diffusion apparatus by sandwiching the scleral tissues between the clamped donor and the receiver chambers. Care was taken to ensure that the epithelial surface of the cornea was towards the donor side. The effective diffusion area was 0.79  $\text{cm}^2$ . A 2 mL volume of ATF (pH, 7.4) was used to fill the receiver chamber and was maintained at a temperature of 35 °C and stirred using a magnetic stirrer. Volumes of the samples (PSLN, SLN and CSLN formulations) equivalent to 1 mg of the drug were placed on the epithelial surface of each cornea in the donor chamber. At predetermined time points, 0.5 mL sample was withdrawn through the sampling port and immediately replaced with an equal volume of preheated ATF solution. Each sample was analyzed with HPLC. The cumulative amounts of drug permeated per unit area of the cornea was calculated using equation (4) [35].

$$Q_n = \frac{V_0}{A} \left[ C_n + \frac{V}{V_0} \sum_{i=1}^{n-1} C_i \right] \quad [4]$$

where  $Q_n$  is the cumulative amount of drug permeated at scheduled time interval,  $V_0$  is the volume of receiver medium,  $V$  is the sampling volume,  $A$  is the effective area of permeation,  $C_n$  is the drug concentration in the receiver medium at different times and  $C_i$  is the drug concentration in the receiver cell before each determination.

A graph of cumulative amount of drug permeated per unit area was plotted against time and the steady state flux across the cornea was obtained from the slope of the regression line of the linear part of the plot. Apparent permeability coefficient was then calculated using equation (5).

$$P_{\text{app}} = \frac{\Delta Q}{\Delta t \times C_0 \times 60} \quad [5]$$

where  $\Delta Q/\Delta t$  is the flux across the corneal tissue,  $C_0$  is the initial concentration of drug in donor compartment, and 60 is taken as the factor to convert hour into minute.

### 2.2.8. Corneal hydration level

The scleral tissues of freshly excised cornea and the corneas used in the permeation study were carefully excised. The corneas were weighed and the weights recorded as  $W_w$ . The corneas were then dried at 70 °C for 12 h and the dry weights taken and recorded as  $W_d$ . The level of corneal hydration (HL %) was calculated using equation (6).

$$\text{HL}(\%) = \left( \frac{W_w - W_d}{W_w} \right) \times 100 \quad [6]$$

### 2.2.9. Data and statistical analysis

All experiments were performed in triplicates for validity of statistical analysis. Results were expressed as mean  $\pm$  SD. ANOVA and Student t-tests were performed on the data sets generated using SPSS software. Differences were considered significant for  $p$  values  $<$  0.05.

## 3. Results and discussion

### 3.1. Box-Behnken design

#### 3.1.1. Experimental design and selection of models

A 3-factor, 3-level design matrix generated by Design Expert® software was used to optimize the formulation parameters. Box-Behnken design (BBD), a 3 factor, 3 level RSM design was used in this study for the development and optimization of the process variables as it requires less experimental runs when compared to other RSM designs such as central composite design. Moreover, several researchers have used BBD to develop and optimize lipid nanoparticles for ocular delivery, thus confirming its validity and usefulness in the optimization process [36, 37].

Box-Behnken design is a cubic design characterized by set of 12 points lying at the midpoint of each edge of a multidimensional cube and five center point replicates giving rise to 17 experimental runs. The 3 independent variables selected were the drug ( $X_1$ ), lipid/polymer ( $X_2$ ), and surfactant ( $X_3$ ); while particle size ( $Y_1$ ) and entrapment efficiency ( $Y_2$ ) were chosen as the dependent responses. The experimental runs, the observed and predicted responses are given in Table S2.

Regression analysis of variance (ANOVA) was used to evaluate the adequacy of the fit models. Quadratic and linear surface response models were found to be adequate for the analysis of the effects of the independent variables on particle size and entrapment efficiency respectively as shown in Table S3.  $P$ -values of  $<$ 0.05 indicate that model terms are significant.

In this case  $X_1$ ,  $X_2$ ,  $X_1X_3$ ,  $X_2X_3$ ,  $X_1^2$ ,  $X_3^2$  are significant model terms for  $Y_1$  while  $X_1$  was the only significant model term for  $Y_2$ . The values greater than 0.1000 indicate the model terms are not significant.

The coefficient represents the expected change in response per unit change in factor value when all remaining factors are kept constant. The intercept in the design represents overall mean response of all the 17 runs. The positive sign before a factor indicates synergistic relationship, while a negative sign indicates an antagonistic relationship between the independent variable and the response. Expressions consisting of more than one factor or higher order term in the regression analysis represent interaction or quadratic relationships, respectively. The coded equation is useful for predicting a response for given levels of each factor; and in identifying the relative impact of the factors by comparing the factor coefficients.

Response surface plots, depicting the effect of independent variables on particle size and entrapment efficiency were plotted. The interaction effects of two independent variables on a response were illustrated graphically using contour plots. As these contour plots can only express two independent variables at a time against the response, the third independent variable is fixed at the center point.

#### 3.1.2. Effects of independent variables on particle size

The particle size for the 17 runs at the levels of the factors tested ranged from 142 to 328 nm with a mean value of 206 nm. It was shown that  $X_1$ ,  $X_2$ ,  $X_1X_3$ ,  $X_2X_3$ ,  $X_1^2$  and  $X_3^2$  were statistically significant parameters ( $p <$  0.05) from the ANOVA test. This means that main, interaction and quadratic effects of the independent variables are all necessary in interpreting their effect on particle size. The quadratic equation generated from the analysis is shown below:

$$\text{Particle size} = 205.8 + 34.25X_1 + 32.25X_2 - 4.75X_3 - 8.25X_1X_2 + 11.75X_1X_3 - 13.75X_2X_3 + 21.225X_1^2 - 8.775X_2^2 + 55.225X_3^2$$

[7]

The positive coefficient of  $X_1$  (drug) indicates a synergistic effect on particle size. This means that increase in the amount of drug increases the particle size. At low level of drug, smaller nanoparticles were produced whereas particle size was higher upon increasing the drug. This is expected because of the high molecular density at the inner phase with increased drug loading. The interaction effect of drug and surfactant was positive. Experimental run 12 with high levels of drug and surfactant gave the highest particle size of 328 nm. The lipid/polymer ratio also had a synergistic effect on particle size as indicated by the high positive coefficient. At the low level of the ratio (0.5), the particle size ranged from 142 to 233 nm, while at high level (0.83), the size range increased to 220–312 nm. The higher the lipid/polymer ratio (i.e. higher lipid content), the higher the viscosity of the dispersion which leads to higher particle size by either decreasing the rate of diffusion of the organic solvent or by resisting the breakdown effect of shear force during stirring [38]. There was a negative interaction effect of lipid/polymer ratio and surfactant on particle size. This means that the effect of lipid/polymer ratio depends on the surfactant concentration; and at high level of surfactant concentration, increasing the ratio can lead to smaller particle sizes. This is because the surfactant provides steric stabilization of the lipid in the aqueous dispersion thereby preventing aggregation of the nanoparticles [39].

The effect of the surfactant on particle size can be understood by the high positive quadratic coefficient. The particle size of the nanoparticles decreased as the concentration of surfactant was increased up to a point

where further increase in surfactant concentration resulted to higher particle sizes. At low level of surfactant, the molecules were insufficient to cover the nanoparticles completely [39]. On increasing the surfactant concentration, the interfacial tension between the lipid and the aqueous phase is decreased leading to the formation and stabilization of smaller nanoparticles. Further increase in surfactant concentration led to increased particle size. This may be a result of a buildup of multiple surfactant layers on the particles and the aggregation of excess surfactant molecules with the nanoparticles. Significant positive interaction effect of surfactant with drug and negative interaction effect of surfactant with lipid polymer ratio on the particle size were observed. This means that at higher lipid polymer ratio, increase in surfactant gave rise to smaller particle size. 3D surface plots showing the interaction effects of the different independent variables on particle size are shown in Fig. 1.

### 3.1.3. Effects of independent variables on entrapment efficiency

The entrapment efficiency (EE) ranged from 93 to 97% for the level combinations used (Table 2), while the mean was 94.7%, according to the model intercept. ANOVA test for the observed encapsulation efficiency percent data indicates that the linear model was significant and fitting for the data. The generated equation in terms of coded values was as follows:

$$\text{Entrapment efficiency} = 94.65 + 1.37X_1 + 0.25X_2 - 0.125X_3 \quad [8]$$

Amount of drug ( $X_1$ ) and lipid polymer ratio ( $X_2$ ) showed positive effects, while surfactant concentration ( $X_3$ ) had a negative effect on entrapment efficiency as seen in Fig. 2. At higher concentrations of the drug, more of the drug was available to be entrapped inside the particles.

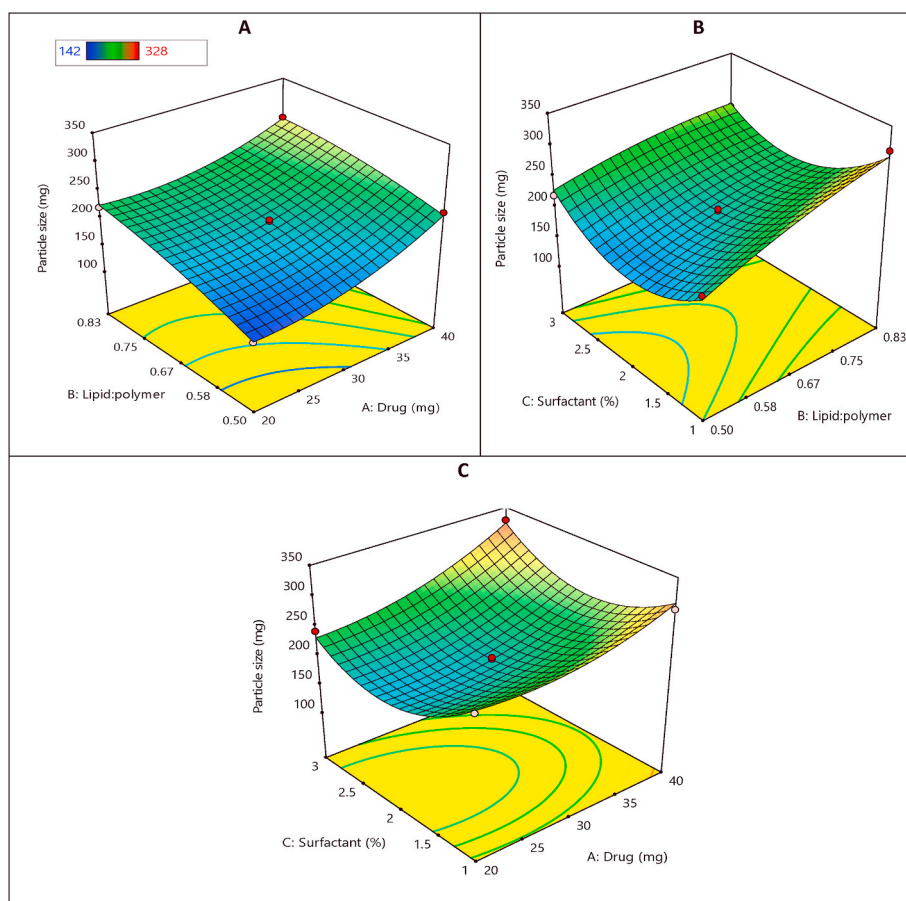


Fig. 1. 3D-response surface plots of the effects of independent variables on particle size: A) lipid/polymer ratio against amount of drug on particle size; B) surfactant concentration against lipid/polymer ratio on particle size; C) surfactant concentration against amount of drug on particle size. The third parameter was kept constant at the center point.

**Table 2**  
Physicochemical result of optimized PSLN, SLN and PSLN.

Formulation	Particle size (nm)	PDI	Zeta potential (mV)	Encapsulation efficiency (%)
Optimized PSLN	141 ± 1	0.193 ± 0.004	-35.6 ± 2.3	93 ± 1
SLN	179 ± 5	0.312 ± 0.042	-30.5 ± 0.4	95 ± 1
CSLN	213 ± 1	0.229 ± 0.004	+24.6 ± 1.1	51 ± 2

This can be used to explain the increase in EE as the drug concentration increases. An opposite effect on the EE was observed with surfactant concentration. This negative effect could be attributed to partition phenomena, as higher concentration of surfactant in the external phase could have increased drug partition from internal to external phase, leading to drug solubilization [40]. The synergistic effect of lipid polymer ratio can be explained by the availability of more space to accommodate the drug molecules. Increase in lipid polymer ratio led to increased viscosity of the dispersion which also reduced the diffusion of the drug to the aqueous phase during formulation. The high entrapment efficiency found with all the formulations can be attributed to the hydrophobic nature of ciprofloxacin.

### 3.1.4. Optimization and validation

The optimized formulation was obtained based on the criteria of entrapment efficiency within the experimental range and minimum particle size. Therefore, a new batch of PSLNs was prepared to validate the reliability of optimization. The composition of the optimum formulation was 20 mg ciprofloxacin, 0.5 lipid/polymer ratio and 2% Tween® 80 with the predicted values as EE 93% and particle size 144 nm. The optimized formulation had a particle size of 141 ± 1 nm and EE of 93.2 ± 0.4%, which was in good agreement with the predicted values, thus indicating the validity and effectiveness of the Box-Behnken design.

## 3.2. Characterization

### 3.2.1. Particle size, polydispersity index (PDI) and zeta potential

The particle size, PDI and zeta potential (ZP) values of the optimized PSLN, SLN and CSLN formulations are shown in Table 2. POZylation of SLN resulted in smaller particle size, lower PDI and higher ZP. Coating the nanoparticles with chitosan gave larger nanoparticles and this could be as a result of adsorption of the chitosan macromolecules on the

particle surface [41]. The differences in the particle sizes of the three batches were significant ( $p < 0.05$ ). All the formulations had a particle size <250 nm, which means that they were suitable for ocular delivery [42]. PDI is a measure of the sample heterogeneity and it is given by the sample particle size distribution. PDI <0.3 is considered optimum, while values < 0.5 are within acceptable limits [43]. The PDI of the formulations were within the acceptable limits.

ZP is a measure of the surface charge of particles and it is an indication of the physical stability of particulate systems. When ZP value is 30 mV and above, the system is considered to be stable due to electrostatic repulsion (Müller et al., 2001). The ZP values of PSLN, SLN and CSLN formulations were -35.6 ± 2.3, -30.5 ± 0.4 and 24.6 ± 1.1 mV, respectively. The high absolute ZP values is an indication of good physical stability of the formulations. The positive ZP of CSLN formulations resulting from the cationic nature of chitosan will favour the interaction between nanoparticles and the negatively charged corneal membranes and consequently increase the residence time of the delivery system [44].

High entrapment efficiency was observed for PSLN and SLN, and a relatively lower EE observed for CSLN (Table 2). The primary determinants of EE are lipid composition and drug solubility. Lipids made up of combination of mono-, di- and triacylglycerols such as Compritol have the ability to accommodate more drug molecules in the spaces created between the carbon chains. The relative hydrophobicity of ciprofloxacin also contributed to the high EE obtained with the formulations.

### 3.2.2. Differential scanning calorimetry

Fig. 3 shows the differential scanning calorimetry (DSC) thermograms of PSLN, SLN and CSLN. CIP and Compritol showed sharp, narrow peaks at 272.88 °C and 72.96 °C with enthalpy of 158.7 J/g and 131.1 J/g, respectively. These peaks represent their melting points and confirm their crystalline nature. For the PSLN (Fig. 3A), the physical mixture, which was composed of ciprofloxacin, Compritol, and PEOx, showed a sharp narrow peak at 71.96 °C with enthalpy of 57.96 J/g, while the optimized POZylated SLN showed a peak at 73.95 °C and enthalpy of 97.75 J/g. For SLN (Fig. 3A), the physical mixture (Compritol and ciprofloxacin) showed a peak at 72.37 °C and another smaller peak at 269.19 °C, which are representative peaks for Compritol and ciprofloxacin, but the lyophilized SLN gave a single endothermic peak at 70.75 °C. For CSLN formulations (Fig. 3C), the physical mixture (ciprofloxacin, Compritol and chitosan) and the lyophilized CSLN gave endothermic melting peaks at 73.90 °C with enthalpy of 112.4 J/g and 69.34 °C with enthalpy of 75.52 J/g, respectively. The summary of this

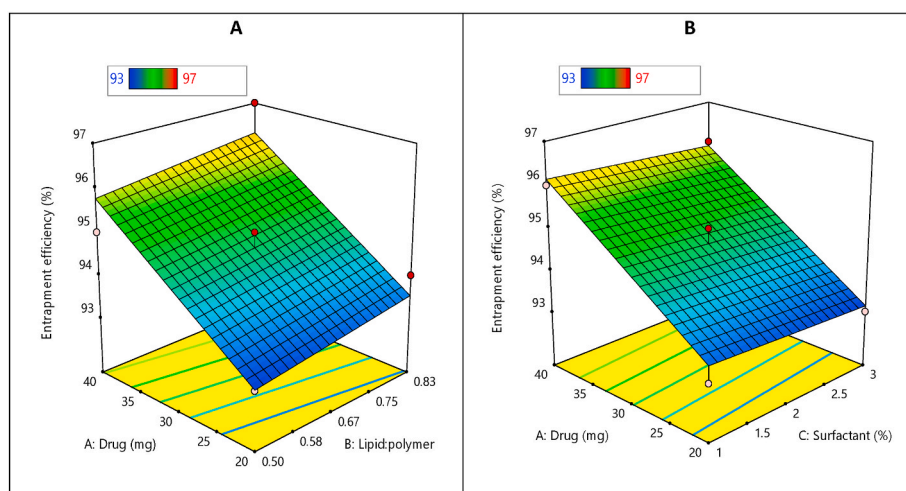


**Fig. 2.** 3D-response surface plots of the effects of independent variables on EE: a) amount of drug against lipid/polymer ratio on entrapment efficiency; b) amount of drug against surfactant concentration on entrapment efficiency. The third parameter was kept constant at the center point.

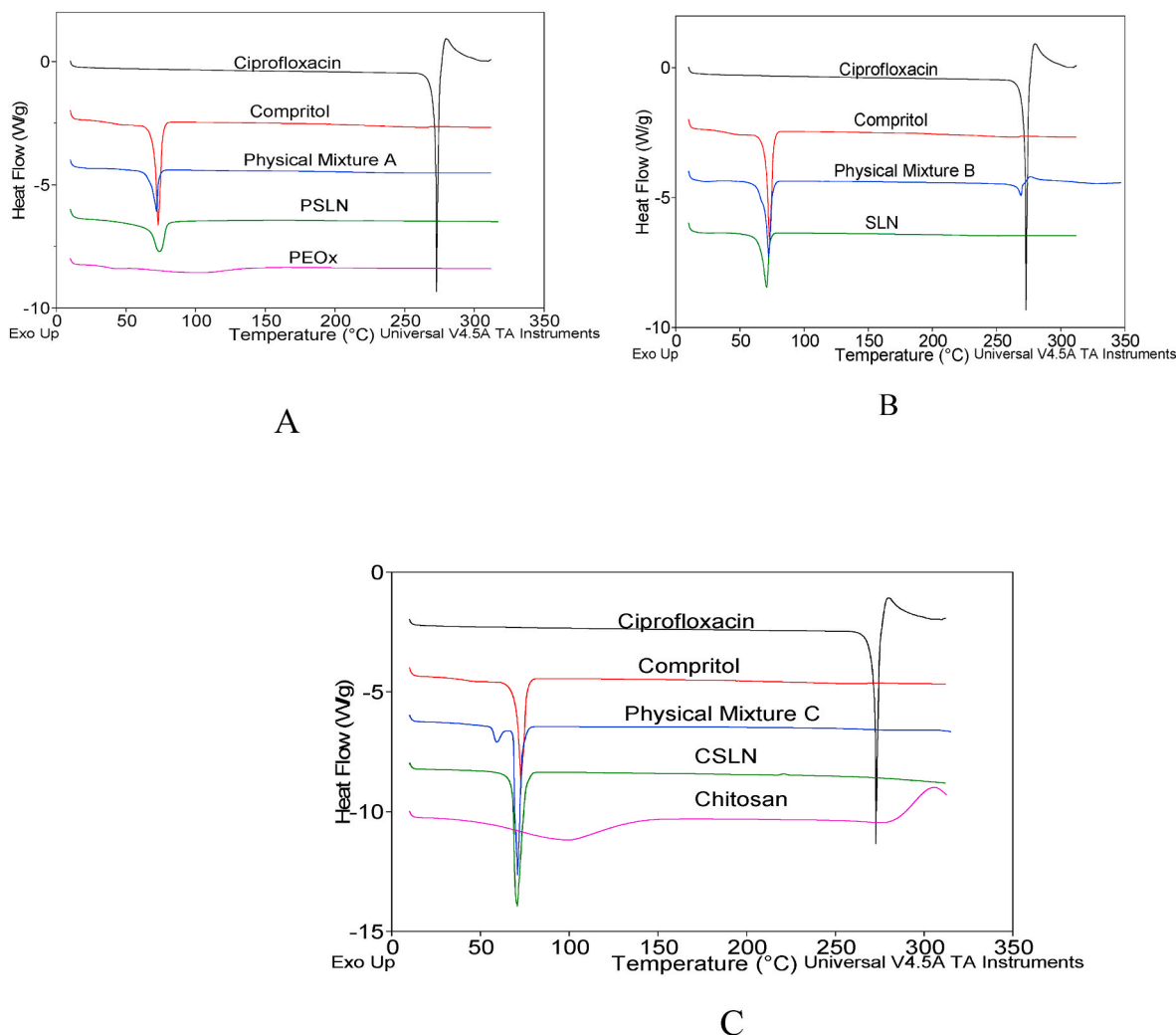


Fig. 3. Overlaid DSC thermograms of A) optimized PSLN B) SLN and C) CSLN.

result is given in Table 3.

A decrease in the enthalpy and height of the melting peaks with the broadening of the peaks of the lyophilized formulations when compared with the pure lipid indicates a decrease in the crystallinity of the lipids. This shows that incorporating lipids in solid lipid nanoparticles led to defects in the crystal lattice structure of the lipid, giving rise to more space for drug entrapment [45]. The disappearance of the CIP melting peak in the DSC thermograms of the formulations is an indication that the drug was molecularly dispersed in the lipid matrix.

### 3.2.3. X-ray diffractometry

The crystallinity of CIP-loaded PSLN, SLN and CSLN was investigated and compared with those of pure CIP, Compritol and physical mixtures of the excipients (Fig. 4) using powdered X-ray diffractometry. CIP X-ray diffractogram showed several sharp, narrow peaks with maximum peak intensity at  $2\theta = 25.47^\circ$  ( $d = 3.49 \text{ \AA}$ ), indicating its crystalline nature. The X-ray diffractogram of Compritol showed only two sharp peaks with the maximum at  $2\theta = 21.42^\circ$  ( $d = 4.14 \text{ \AA}$ ). In the case of PSLN physical mixture, three major peaks were observed with the maximum peak at  $2\theta$

**Table 3**  
DSC and XRD characterization of the formulations.

Parameters	Compritol	Ciprofloxacin	PSLN		SLN		CSLN	
			Mixture Physical	Lyophilized PSLN	Mixture Physical	Lyophilized SLN	Physical Mixture	Lyophilized CSLN
<b>DSC</b>								
Melting peak ( $^\circ\text{C}$ )	72.96	272.88	71.96	73.95	72.37, 269.19	70.75	73.90	69.34
Enthalpy (J/g)	131.3	158.7	57.96	97.75	112, 14.74	81.11	112.4	75.52
<b>X-ray</b>								
$2\theta$ of maximum intensity ( $^\circ$ )	21.42	25.47	21.55	19.62	21.40	19.59	21.50	21.58
Corresponding d-spacing ( $\text{\AA}$ )	4.14	3.49	4.12	4.52	4.15	4.52	4.13	4.12
Crystallinity (%)	43.41	80.58	32.35	20.37	53.03	37.87	22.72	14.50

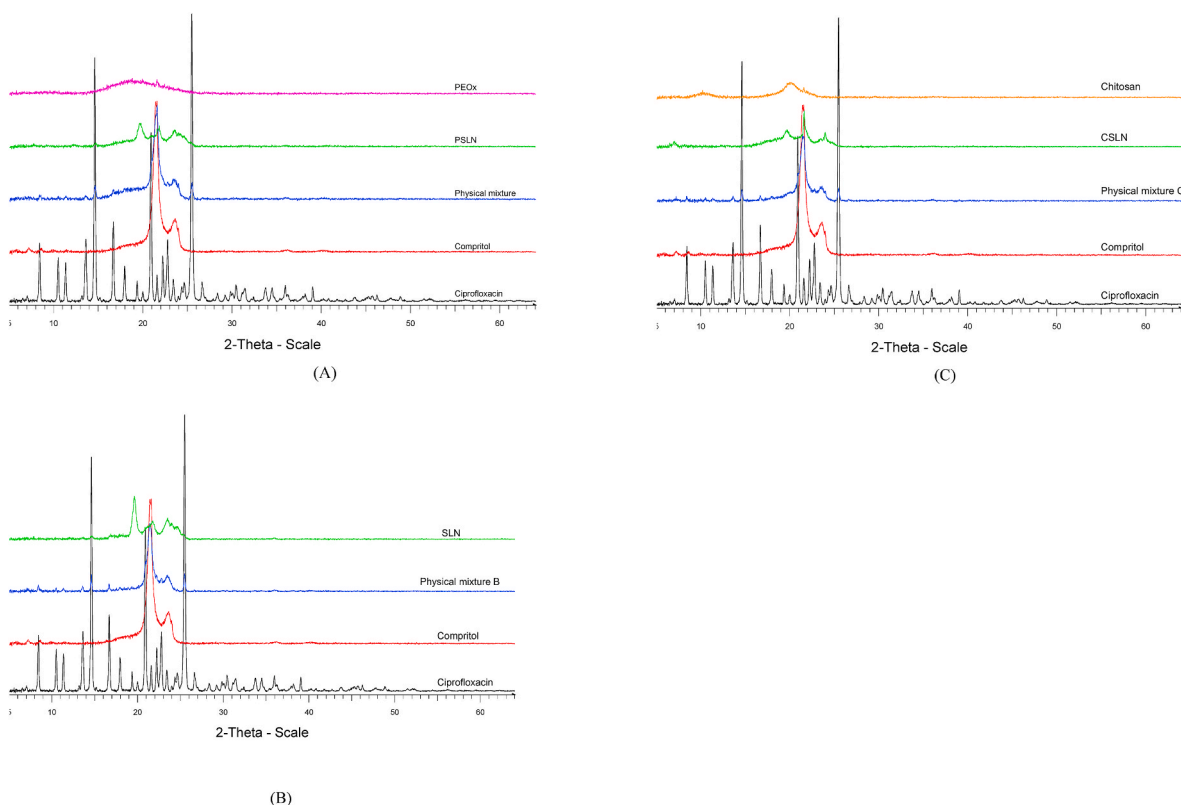


**Fig. 4.** X-ray diffraction patterns of (A) ciprofloxacin, Compritol, PEOx, physical mixture of excipients and lyophilized PSLN; (B) ciprofloxacin, Compritol, physical mixture of excipients and lyophilized SLN; and (C) ciprofloxacin, Compritol, chitosan, physical mixture of excipients and lyophilized CSLN formulations.

= 21.55° ( $d = 4.12 \text{ \AA}$ ), which represented an overlapped peak of both CIP and Compritol. The major peaks for ciprofloxacin and Compritol were visible but with reduced intensities. The diffractogram of the lyophilized PSLN gave three major peaks. The major peaks for CIP disappeared from the diffraction pattern of the lyophilized PSLN indicating its amorphous state in the formulation. In other words, CIP was successfully entrapped in the core of the lipid. The overlaid diffractograms of SLN and CSLN showed similar result as that of PSLN. The peaks of maximum intensities were at  $2\theta = 19.59^\circ$  ( $d = 4.53 \text{ \AA}$ ) and  $2\theta = 21.58^\circ$  ( $d = 4.12 \text{ \AA}$ ) for lyophilized SLN and CSLN, respectively. However, three major peaks were observed for both between  $2\theta = 19.5^\circ$  and  $2\theta = 24^\circ$ . The sharp decrease in the peak intensities of the lyophilized PSLN, SLN and CSLN when compared to that of Compritol indicates a marked decrease in the crystallinity of the formulations. The calculated crystallinities for CIP, Compritol, lyophilized PSLN, SLN and CSLN were 80.58%, 43.41%, 20.37%, 37.87% and 14.50%, respectively. This decrease in crystallinities of the formulations confirms previous result from DSC analysis, meaning that there would be enough space where drug would be incorporated compared to the pure lipid.

### 3.2.4. Transmission electron microscopy (TEM)

Transmission electron microscopy was used to investigate the morphology of the formulations. The micrographs of the formulations (Fig. 5) showed well-identified spherical polymer-coated structures with sizes consistent with the data of the particle size analysis using dynamic light scattering. The fused nanoparticles present in the micrographs may be due to the sample preparation process before the analysis.

### 3.3. In vitro release study

For a drug to exert any pharmacological action, it has to leave the drug product and diffuse into the surrounding biological medium. The release of CIP from the formulation was investigated and the summary of

the result is shown in Fig. 6. The cumulative amounts of drug released from optimized PSLN, SLN and CSLN after 24 h were  $73 \pm 3\%$ ,  $75 \pm 1\%$  and  $71 \pm 3\%$ , respectively. There was initial burst release of CIP followed by gradual release which was sustained for 24 h for all the formulations. This release pattern is similar to what we got in our previous paper on the permeation of lipid based microsuspension [6]. The initial burst release, which is attributed to free or loosely bound drug, was higher with CSLN formulation as there was more than 30% cumulative drug release within the first 2 h. This correlates with its lower entrapment efficiency giving rise to higher concentration of free drug.

The mechanism and kinetics of drug release was investigated by the model dependent method using DDSolver Excel add-in application. The parameters used in assessing the model with the best fit were  $R^2_{\text{adjusted}}$ , MSC, and AIC and the result obtained is shown in Table 4. Korsmeyer-Peppas model was considered the best model that described the release mechanism for all the formulations because of the higher  $R^2_{\text{adjusted}}$ , lower AIC and higher MSC when compared to other models.

The release exponent ( $n$ ) values for the Korsmeyer-Peppas model is also shown in Table 4. All the formulations showed Fickian diffusion as  $n < 0.45$ . This means that the drug release from these nanoparticles was through the process of diffusion of the drug [30].

### 3.4. Mucoadhesion study

From the result of mucoadhesion study shown in Fig. 7 (a and b), CSLN showed the greatest muco-adhesiveness to the porcine cornea, followed by SLN and PSLN. Because of the positive charge of CSLN, there is electrostatic interaction between the molecules and the negatively charged ocular surface leading to decrease in tear wash out rate and consequently higher retention on the ocular surface. The mucoadhesive property of chitosan is well documented in literature [12,46]. The retention of SLN and PSLN formulations by the ocular tissue though not as high as CSLN was significant when compared to the negative control

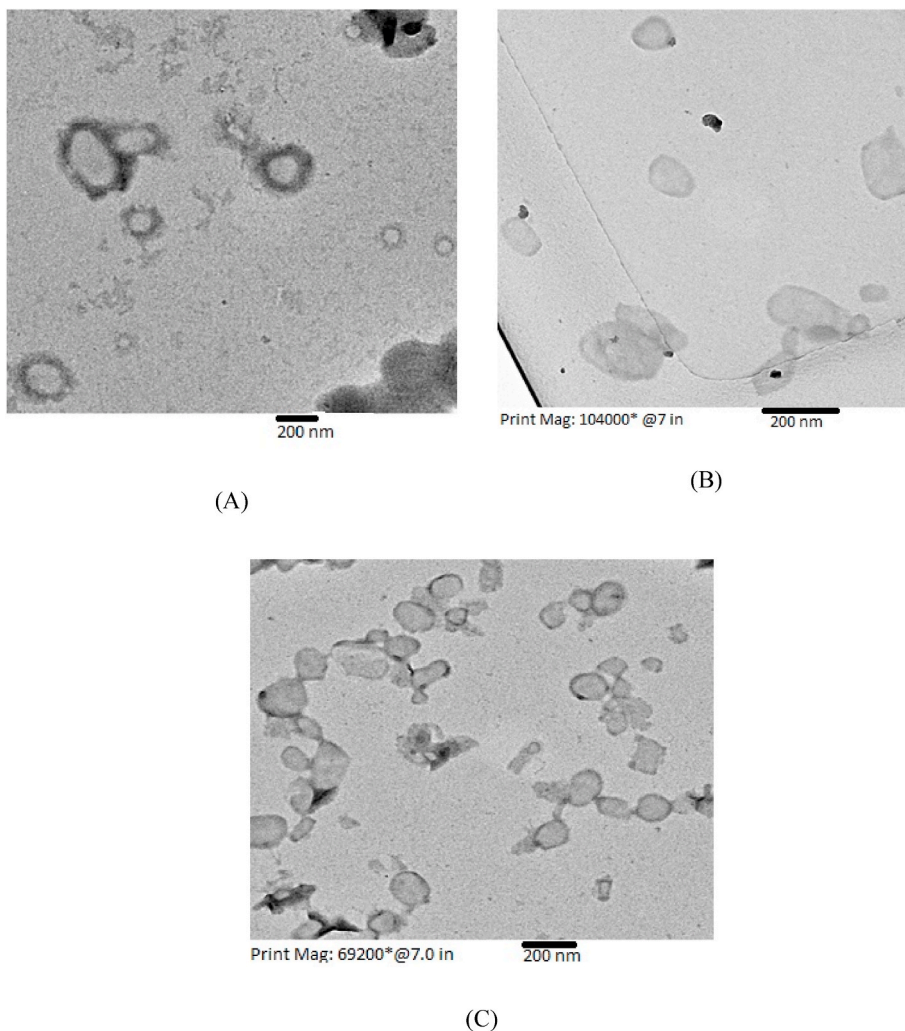


Fig. 5. Transmission electron micrographs of A) optimized PSLN formulation B) SLN C) CSLN.

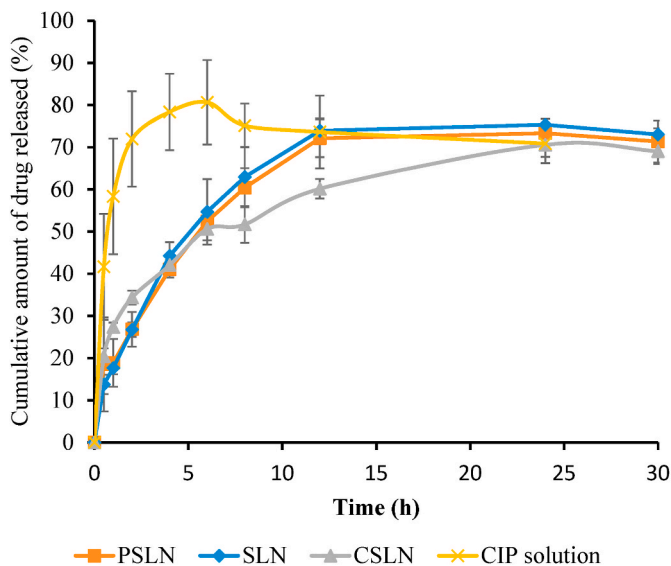


Fig. 6. In vitro drug release of CIP from different formulations.

( $p < 0.05$ ). This is in agreement with report from several researchers as presented in a review by Sánchez-López et al. [10] on the mucoadhesive properties of nanoparticles, which has been attributed to their nanosize and increased surface area. Fig. 7 (a and b) clearly showed higher fluorescence intensity of CSLN-treated excised cornea after washing the surface with 10 mL of ATF compared with SLN and PSLN. This means higher retention of CSLN on the corneal surface.

### 3.5. Ex vivo corneal permeation study

The corneal tissues present great barrier to ocular drug permeation because of the biphasic nature of the layers and the presence of tight junctions. The permeation of ciprofloxacin from the formulations through porcine cornea was evaluated and the results are shown in Fig. 8. Permeation parameters such as steady state flux and permeability coefficient were evaluated for the formulations and the result shown in Table 5. There was significant linear permeation of the drug from the formulations through the porcine cornea. CSLN formulations showed more permeation than the PSLN and SLN formulations and exhibited approximately 2-fold greater flux than PSLN and SLN. This may be as a result of the ability of chitosan to reversibly disrupt the tight junctions of the corneal epithelium thereby enhancing drug permeation.

The corneal hydration level (HL) is a parameter commonly used to evaluate damage to cornea tissue. The normal range of HL (%) is 76–80%. A value above 83% denotes damages to the cornea epithelium or endothelium [47]. As shown in Table 5, the corneal hydration values

**Table 4**  
Kinetics and mechanism of release parameters for nanoparticle formulations.

Models	PSLN				SLN				CSLN			
	R <sup>2</sup> _adj.	n	AIC	MSC	R <sup>2</sup> _adj.	n	AIC	MSC	R <sup>2</sup> _adj.	n	AIC	MSC
Zero order	0.245	–	77	–0.3	0.303	–	77	–0.2	–0.099	–	77	–0.9
First order	0.868	–	61	1.4	0.911	–	59	1.9	0.614	–	68	0.2
Higuchi	0.903	–	58	1.7	0.907	–	59	1.8	0.842	–	60	1.1
Korsmeyer-Peppas	0.942	0.38	54	2.2	0.931	0.39	57	2.0	0.994	0.30	30	4.3

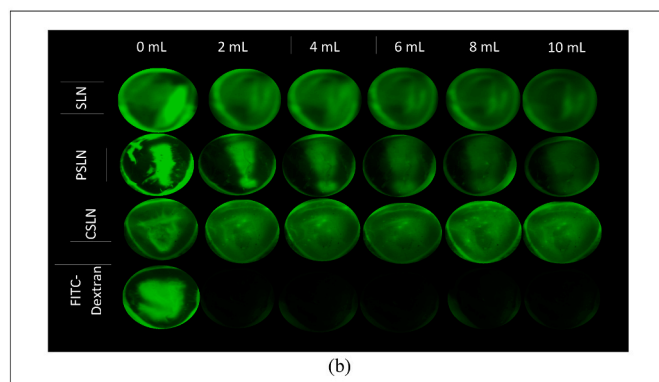
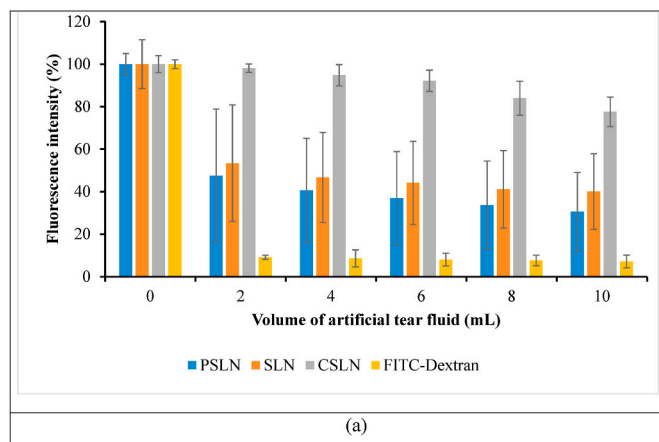


**Fig. 7.** (a) Fluorescence intensity values as a function of ATF volume and (b) Fluorescence images showing the retention of PSLN, SLN and CSLN on porcine cornea after washing with different volume of artificial tear fluid.

after the permeation studies for all the formulations were not higher than 83%. This is an indication that the formulations did not cause any damage to the corneal tissue during the studies.

#### 4. Conclusion

Ciprofloxacin-loaded POZylated and chitosan-coated solid lipid nanoparticles were successfully developed using Compritol as the lipid, Tween 80 as the surfactant and poly(2-ethyl-2-oxazoline) or chitosan as the polymer coating. An optimized formulation was obtained using Box-Behnken design. The results obtained from the study showed that the formulations have the potential to improve ocular drug delivery. SLN coated with chitosan exhibited higher mucoadhesion and retention on corneal tissues compared with POZylated SLN and also showed higher flux and apparent permeability, but with lower entrapment efficiency. Future research may include in vivo testing of the formulations developed in this work.

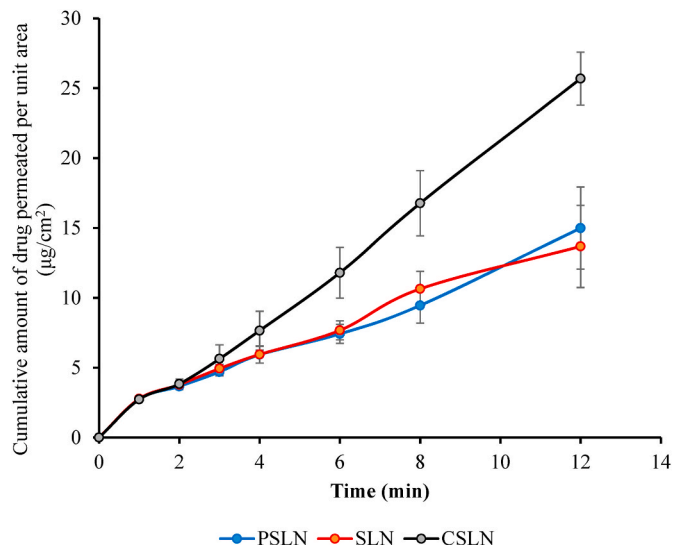


**Fig. 8.** Corneal permeation of ciprofloxacin from optimized PSLN, SLN and CSLN through porcine cornea.

**Table 5**  
Corneal permeation parameters.

	Steady state flux ( $\mu\text{g}/\text{cm}^2/\text{h}$ )	Apparent permeability coefficient ( $\text{cm}/\text{min}$ ) $\times 10^{-5}$	Hydration level (%)
PSLN	$0.95 \pm 0.16$	$1.59 \pm 0.27$	$79.0 \pm 3.0$
SLN	$1.01 \pm 0.28$	$1.69 \pm 0.46$	$78.0 \pm 5.0$
CSLN	$2.27 \pm 0.06$	$3.79 \pm 0.10$	$80.0 \pm 1.7$
Control (untreated cornea)	–	–	$78.0 \pm 1.5$

#### CRedit roles

Adaeze L. Onugwu (Investigation, Methodology, Writing - original draft), Anthony A. Attama (Supervision, Funding acquisition, Writing - original draft, Writing - review & editing), Petra O. Nnamania (Investigation), Sabastine O. Onugwu (investigation), Ebele B. Onuigbo (investigation), Vitaliy V. Khutoryanskiy (Conceptualization, Supervision, Funding acquisition, Writing - review & editing).

#### Funding

This work was partly sponsored by the Commonwealth Scholarship Commission, United Kingdom through a Split-site Scholarship award (Ref: NGCN-2018-244) to Adaeze Linda Onugwu.

#### Declaration of competing interest

The authors declare that they have no known competing financial interests or personal relationships that could have appeared to influence the work reported in this paper.

## Appendix A. Supplementary data

Supplementary data to this article can be found online at <https://doi.org/10.1016/j.jddst.2022.103527>.

## References

- [1] A. Patel, K. Cholkar, V. Agrahari, A.K. Mitra, Ocular drug delivery systems: an overview, *World J. Pharmacol.* 2 (2013) 47–64.
- [2] J. Shen, G.W. Lu, P. Hughes, Targeted ocular delivery with pharmacokinetic/pharmacodynamics considerations, *Pharm. Res.* (N. Y.) 35 (2018) 217–237.
- [3] A. Pavankumarreddy, S. Parthiban, A. Vikneswari, G.P. Senthikumar, Evaluation of potential antimicrobial activity of levofloxacin loaded solid lipid nanoparticles, *Asian J. Res. Biol. Pharm. Sci.* 2 (2014) 99–111.
- [4] R.C. Nagarwal, S. Kant, P.N. Singh, P. Maiti, J.K. Pandit, Polymeric nanoparticulate system: a potential approach for ocular drug delivery, *J. Contr. Release* 136 (2009) 2–13.
- [5] Ü.N. Okur, H.E. Gökçe, D.İ. Bozbiyık, S. Eğrilmez, Ö. Özer, G. Ertan, Preparation and in vitro–in vivo evaluation of ofloxacin loaded ophthalmic nano structured lipid carriers modified with chitosan oligosaccharide lactate for the treatment of bacterial keratitis, *Eur. J. Pharmaceut. Sci.* 63 (2014) 204–215.
- [6] A.L. Onugwu, C.P. Agbo, C.S. Nwagwu, S.E. Uzundu, A.C. Echezona, J. D. Nwabueze Ogbonna, F.C. Kenchukwu, C.E. Umeyor, E.M. Uronnachi, P. A. Akpa, M.A. Momoh, P.O. Nnamani, C.C. Müller-Goymann, A.A. Attama, Development of lipid-based microemulsions for improved ophthalmic delivery of gentamicin sulphate, *Ther. Deliv.* 12 (9) (2021) 671–683.
- [7] R. Shah, D. Eldrige, E. Palombo, I. Harding, *Lipid Nanoparticles: Production, Characterization and Stability*, Springer International Publishing, New York, 2015, pp. 11–22.
- [8] E.B. Souto, R.H. Müller, Lipid nanoparticles: effect on bioavailability and pharmacokinetic changes, *Handb. Exp. Pharmacol.* 197 (2010) 115–141.
- [9] C.C. Müller-Goymann, Physicochemical characterization of colloidal drug delivery systems such as reverse micelles, vesicles, liquid crystals and nanoparticles for topical administration, *Eur. J. Pharm. Biopharm.* 58 (2004) 343–356.
- [10] E. Sánchez-López, M. Espina, S. Doktorovova, E.B. Souto, M.L. García, Lipid nanoparticles (SLN, NLC): overcoming the anatomical and physiological barriers of the eye-Part II - ocular drug-loaded lipid nanoparticles, *Eur. J. Pharm. Biopharm.* 110 (2017) 58–69.
- [11] I.A. Sogias, A.C. Williams, V.V. Khutoryanskiy, Why is chitosan mucoadhesive? *Biomacromolecules* 9 (2008) 1837–1842.
- [12] L. Duxfield, R. Sultana, R. Wang, V. Englebretsen, S. Deo, S. Swift, R. Al-Kassas, Development of gatifloxacin-loaded cationic polymeric nanoparticles for ocular drug delivery, *Pharmaceut. Dev. Technol.* 21 (2016) 172–179.
- [13] D. Vilasaliu, R. Exposito-Harris, A. Heras, L. Casettari, M. Garnett, L. Illum, S. Stolnik, Tight junction modulation by chitosan nanoparticles: comparison with chitosan solution, *Int. J. Pharm.* 400 (2010) 183–193.
- [14] J. Zhang, X. Zhu, Y. Jin, W. Shan, Y. Huang, Mechanism study of cellular uptake and tight junction opening mediated by goblet cell-specific trimethyl chitosan nanoparticles, *Mol. Pharm.* 11 (2014) 1520–1532.
- [15] J.S. Suk, Q. Xu, N. Kim, J. Hanes, L.M. Ensign, PEGylation as a strategy for improving nanoparticle-based drug and gene delivery, *Adv. Drug Deliv. Rev.* 99 (2016) 28–51.
- [16] N.N. Porfiryeva, R.I. Moustafine, V.V. Khutoryanskiy, PEGylated systems in pharmaceuticals, *Polym. Sci. Series C* 62 (2020) 62–74.
- [17] K. Knop, R. Hoogenboom, D. Fischer, U.S. Schubert, Poly (ethylene glycol) in drug delivery: pros and cons as well as potential alternatives, *Angew. Chem., Int. Ed. Engl.* 49 (2010) 6288–6308.
- [18] R. Hoogenboom, Poly(2-oxazoline)s: a polymer class with numerous potential applications, *Angew. Chem. Int. Ed.* 48 (2009) 7978–7994.
- [19] M. Barz, R. Luxenhofer, R. Zentel, M.J. Vicent, Overcoming the PEG-addiction: well-defined alternatives to PEG, from structure–property relationships to better defined therapeutics, *Polym. Chem.* 2 (2011) 1900–1918.
- [20] K. Lava, B. Verbracken, R. Hoogenboom, Poly(2-oxazoline)s and click chemistry: a versatile toolbox toward multi-functionalized polymers, *Eur. Polym. J.* 65 (2015) 98–111.
- [21] H. Wei, C. Yu, Cyclodextrin-functionalized polymers as drug carriers for cancer therapy, *Biomater. Sci.* 3 (2015) 1050–1060.
- [22] E.D.H. Mansfield, V.R. Rosa, R.M. Kowalczyk, I. Grillo, R. Hoogenboom, K. Silence, P. Hole, A.C. Williams, V.V. Khutoryanskiy, Side chain variations radically alter the diffusion of poly (2-alkyl-2-oxazoline) functionalised nanoparticles through a mucosal barrier, *Biomater. Sci.* 4 (2016) 1318–1327.
- [23] H. Yuan, L. Wang, Y. Du, J. You, F. Hu, S. Zeng, Preparation and characteristics of nanostructured lipid carriers for control-releasing progesterone by melt-emulsification, *Colloids Surf. B Biointerfaces* 60 (2007) 174–179.
- [24] P.K. Gaur, S. Mishra, S. Purohit, Solid lipid nanoparticles of Guggul lipid as drug carrier for transdermal drug delivery, *BioMed Res. Int.* (2013) 1–10.
- [25] S.R.S. Rudrangi, R. Bhomia, V. Trivedi, G.J. Vine, J.C. Mitchell, B.D. Alexander, S. R. Wicks, Influence of the preparation method on the physicochemical properties of indomethacin and methyl- $\beta$ -cyclodextrin complexes, *Int. J. Pharm.* 479 (2015) 381–390.
- [26] S.O. Tanjinatus, H.I. Ahsanul, D. Irin, S.M. Ashraful Islam, Comparative in vitro dissolution study of some ciprofloxacin generic tablets under biowaiver conditions by RP-HPLC, *Int. J. Pharma Sci. Res.* 2 (2011) 3129–3135.
- [27] M. Kamran, A. Ahad, M. Aqila, S. Imam, Y. Sultana, A. Ali, Design, formulation and optimization of novel soft nano-carriers for transdermal olmesartan medoxomil delivery: in vitro characterization and in vivo pharmacokinetic assessment, *Int. J. Pharm.* 505 (2016) 147–158.
- [28] G.A. Shazly, Ciprofloxacin controlled-solid lipid nanoparticles: characterization, in vitro release, and antibacterial activity assessment, *BioMed Res. Int.* 2017 (2017) 1–9.
- [29] T. Higuchi, Mechanism of sustained-action medication, *J. Pharmacol. Sci.* 52 (12) (1963) 1145–1149.
- [30] R.W. Kormeyer, R. Gurny, E. Doelker, P. Buri, N.A. Peppas, Mechanisms of solute release from porous hydrophilic polymers, *Int. J. Pharm.* 15 (1983) 25–35.
- [31] N.A. Peppas, Analysis of Fickian and non-Fickian drug release from polymers, *Pharm. Acta Helv.* 60 (1985) 110–111.
- [32] Y. Zhang, M. Huo, J. Zhou, A. Zou, W. Li, C. Yao, S. Xie, DDSolver: an add-in program for modeling and comparison of drug dissolution profiles, *AAPS J.* 12 (3) (2010) 263–271.
- [33] J. Zuo, Y. Gao, N. Bou-Chacra, R. Löbenberg, Evaluation of the DDSolver software applications, *BioMed Res. Int.* 2014 (2014).
- [34] E.A. Mun, A.C. Williams, V.V. Khutoryanskiy, Adhesion of thiolated silica nanoparticles to urinary bladder mucosa: effects of PEGylation, thiol content and particle size, *Int. J. Pharm.* 512 (2016) 32–38.
- [35] J. Ban, Y. Zhang, X. Huang, G. Deng, D. Hou, Y. Chen, Z. Lu, Corneal permeation properties of a charged lipid nanoparticle carrier containing dexamethasone, *Int. J. Nanomed.* 12 (2017) 1329–1339.
- [36] F. Wang, M. Zhang, D. Zhang, Y. Huang, L. Chen, S. Jiang, K. Shi, R. Li, Preparation, optimization, and characterization of chitosan coated solid lipid nanoparticles for ocular drug delivery, *J. Biomed. Res.* 32 (2018) 411–423.
- [37] H.M. Eid, M.H. Elkomy, S.F. El Menhaweh, H.F. Salem, Development, optimization, and in vitro/in vivo characterization of enhanced lipid nanoparticles for ocular delivery of ofloxacin: the influence of pegylation and chitosan coating, *AAPS PharmSciTech* 20 (2019) 183.
- [38] P.M. Kashif, A. Madni, M. Ashfaq, M. Rehman, M.A. Mahmood, M.I. Khan, N. Tahir, Development of Eudragit RS 100 microparticles loaded with ropinirole: optimization and in vitro evaluation studies, *AAPS PharmSciTech* 18 (2016) 1810–1822.
- [39] T. Helgason, T.S. Awad, K. Kristbergsson, D.J. McClements, J. Weiss, Effect of surfactant surface coverage on formation of solid lipid nanoparticles (SLN), *J. Colloid Interface Sci.* 334 (2009) 75–81.
- [40] M. Ferreira, L.L. Chaves, S.C. Lima, S. Reis, Optimization of nanostructured lipid carriers loaded with methotrexate: a tool for inflammatory and cancer therapy, *Int. J. Pharm.* 492 (2015) 65–72.
- [41] S. Mohammadi-Samani, R. Miri, M. Salmanpour, N. Khalighian, S. Sotoudeh, N. Erfani, Preparation and assessment of chitosan-coated superparamagnetic Fe<sub>3</sub>O<sub>4</sub> nanoparticles for controlled delivery of methotrexate, *Res. Pharm. Sci.* 8 (2013) 25–33.
- [42] A. Zimmer, J. Kreuter, Microspheres and nanoparticles used in ocular delivery systems, *Adv. Drug Deliv. Rev.* 16 (1995) 61–73.
- [43] E.J. Cho, H. Holback, K.C. Liu, S.A. Abouelmagd, J. Park, Y. Yeo, Nanoparticle characterization: state of the art, challenges, and emerging technologies, *Mol. Pharm.* 10 (6) (2013) 2093–2110.
- [44] P.S. Apaolaza, D. Delgado, A.D. Pozo-Rodríguez, A.R. Gascon, M.A. Solinis, A novel gene therapy vector based on hyaluronic acid and solid lipid nanoparticles for ocular diseases, *Int. J. Pharm.* 465 (2014) 413–426.
- [45] A.A. Attama, S. Reichl, C.C. Müller-Goymann, Diclofenac sodium delivery to the eye: in vitro evaluation of novel solid lipid nanoparticle formulation using human cornea construct, *Int. J. Pharm.* 355 (2008) 307–313.
- [46] A. Khare, K. Grover, P. Pawar, I. Singh, Mucoadhesive polymers for enhancing retention in ocular drug delivery, *Progress in adhesion and adhesives* (2015) 451–484.
- [47] R.D. Schoenwald, H.S. Huang, Corneal penetration behavior of  $\beta$ -blocking agents: physical chemical factors, *J. Pharmacol. Sci.* 72 (1983) 1266–1272.
- [48] I. Krtalić, S. Radošević, A. Hafner, M. Grassi, M. Nenadić, B. Cetina-Čizmek, J. Filipović-Gričić, I. Pepić, J. Lovrić, D-optimal design in the development of rheologically improved in situ forming ophthalmic gel, *J. Pharmaceut. Sci.* 107 (6) (June 2018) 1562–1571, <https://doi.org/10.1016/j.xphs.2018.01.019>.